



Article

Study of the Response of Environmental Factors of the Coastal Area in Zhoushan Fishery to Typhoon In-fa Based on Remote Sensing

Rong Tang ^{1,2} , Lina Cai ^{1,2,*}, Xiaojun Yan ¹ , Xiaomin Ye ², Yuzhu Xu ² and Jie Yin ¹¹ Marine Science and Technology College, Zhejiang Ocean University, Zhoushan 316004, China² Key Laboratory of Space Ocean Remote Sensing and Application, Ministry of Natural Resources, Beijing 100081, China

* Correspondence: clnown@zjou.edu.cn

Abstract: The response of typical environmental factors in Zhoushan Fishery, including sea surface temperature (SST), sea surface salinity (SSS), and chlorophyll *a* (Chl-*a*), before and after Typhoon In-fa was analyzed using satellite data and reanalysis data in this study. Additionally, this study simultaneously elucidated the mechanism by which the typhoon affected these factors. The results showed that: (1) the strong vertical mixing caused by In-fa provoked a decrease in SST, while the asymmetric typhoon wind stress and vertical difference in temperature structure before the typhoon caused a more robust cooling of SST on the right side of the In-fa track; (2) despite the strong mixing and inflow of hypersaline seawater increasing SSS, the combined effect of intense rainfall and diluted water inflow caused an overall decrease in SSS after In-fa's landing; (3) In-fa caused the Chl-*a* concentration to decrease first and then increase. The high cloudiness and low Chl-*a* seawater inflow inhibited the phytoplankton growth during the typhoon, while the abundant light, rich surface nutrients under the upwelling effect, and transport of rich land-based substances induced rapid phytoplankton reproduction after the typhoon; and (4) the change in Chl-*a* concentration, current, temperature, and salinity induced by a typhoon are essential factors that affect fish behavior and community composition in fisheries. This study provides a point of reference to reveal the response of environmental factors to typhoons and their effects on fishery resources in fisheries located on nearshore estuarine shallow waters with intensive islands.

Keywords: typhoon; Zhoushan Fishery; environmental factors; fishery resource

Citation: Tang, R.; Cai, L.; Yan, X.; Ye, X.; Xu, Y.; Yin, J. Study of the Response of Environmental Factors of the Coastal Area in Zhoushan Fishery to Typhoon In-fa Based on Remote Sensing. *Remote Sens.* **2023**, *15*, 3349. <https://doi.org/10.3390/rs15133349>

Academic Editors: Magaly Koch, Zhixiang Fang, Yukiharu Hisaki, Jaroslaw Teğowski and Quanyi Huang

Received: 31 May 2023
Revised: 23 June 2023
Accepted: 26 June 2023
Published: 30 June 2023



Copyright: © 2023 by the authors. Licensee MDPI, Basel, Switzerland. This article is an open access article distributed under the terms and conditions of the Creative Commons Attribution (CC BY) license (<https://creativecommons.org/licenses/by/4.0/>).

1. Introduction

Typhoons (tropical cyclones or storms) are a common oceanic phenomenon. Among the numerous typhoons, about 6.5 of them pass by the eastern coast of China [1,2], making it one of the most frequent natural disasters in this area. The transit of typhoons can cause dramatic disturbances to the marine environment, causing varying degrees of change to the marine environment, climate, and ecosystems [3,4]. A crucial concern has been the response of the ocean to environmental factors.

Temperature, salinity, and chlorophyll *a* (Chl-*a*) responses to typhoon events have been extensively studied in the northwest Pacific Ocean (NOP). Numerous studies have demonstrated that strong winds induce ocean cooling during typhoons through vertical entrainment processes, resulting in sea surface temperature (SST) decreases ranging from 1 to 10.8 °C [5–8]. Substantial rainfall from tropical cyclones can reduce sea surface salinity (SSS). At the same time, evaporation, mixing, and Ekman pumping can increase SSS. The different responses of SSS to typhoons may result from variations in the strength of the effects of the four processes [4,9].

The location, depth, and duration of the subsurface chlorophyll maximum layer (SCML) are controlled by processes such as intense mixing, upwelling, and entrainment

induced by strong winds. These processes also significantly contribute to increased phytoplankton biomass in the upper ocean [10,11]. In coastal waters, abundant rainfall and runoff can cause a substantial influx of nutrients from terrestrial sources, and it is coupled with advection transport, which results in coastal phytoplankton blooms [12–14].

Estuaries and nearshore waters serve as concentration zones for land–sea interaction, where physical, chemical, biological, and geological processes are coupled and variable, contributing to a sensitive and fragile ecological environment [15]. Typhoons cause significant disruptions to the maritime environment, leading to increased estuary runoff, reduced dissolved oxygen, water clarity and temperature changes, and other factors that may impact fish communities [16,17]. These disturbances can directly alter aquatic habitats, potentially resulting in the escape and mortality of marine organisms [18,19]. Conversely, the enhanced primary productivity in the estuary can increase fishery production [20,21].

Due to global warming, typhoons in the NOP have become more frequent and intense [22,23]. Based on the critical relationship between spatial movement, community and density of fish, and changes in aquatic habitats, typhoons by no means have a negligible impact on habitat elements and marine organisms within the fishery. Until now, studies have examined changes in fish biomass density and species richness in the outer sea [24], nearshore waters (estuaries, bays, coral reef areas) [17,19,20], and their inland watersheds [25] after typhoons.

Zhoushan Fishery is adjacent to the Yangtze River estuary, Hangzhou Bay, the Yellow Sea, and the East China Sea, serving as the convergence point for various runoff currents (Yangtze diluted water (YDW), Qiantang River) and sea currents (Taiwan warm current (TWC), Subei coastal current, Zhemin coastal current (ZMCC)). There are special geographical conditions, and the fishery ecosystem contributes to the area being the most significant and excellent fishery in China [26,27]. However, the area is also more frequently affected by typhoons, posing a threat to the stability of the estuary and to the habitat of Zhoushan Fishery. Given that the environmental conditions of fisheries in each sea area and the characteristics of transiting typhoons are very different [28], there is a lack of research on the effects of typhoons on Zhoushan Fishery in the northwest part of the East China Sea, and this needs to be further explored.

Typhoon effects on the ocean and shelf marine environment have been primarily studied in the past using data from ocean buoys [29], remote sensing observations [30,31], numerical simulations [9,32], and combinations of in situ observations and numerical simulations [33,34]. However, the rapid changes in the path and intensity of typhoons make it challenging to achieve large-scale, simultaneous sampling due to the high cost of setting up buoys and conducting cruise measurements as well as the low temporal resolution [29]. Moreover, technical problems with single satellite data, such as missing values due to cloud cover [35] and the low temporal resolution of the dataset [36], can result in a lack of observational information during typhoon transit. To overcome these limitations, reanalysis products that combine in situ observation sites, multi-source satellite remote sensing observations, and numerical simulations provide an effective method [34,37] that offers more comprehensive and systematic spatial and temporal information for periods of severe conditions like typhoons.

In the study, based on the remote sensing data from the Moderate Resolution Imaging Spectroradiometer (MODIS) and Gaofen-4 (GF-4) satellite as well as reanalysis products, which was combined with a comparison of environmental factors in the fishery before and after a typhoon, we revealed the response characteristics and influence mechanisms of SST, SSS, and Chl-*a*, typical environmental factors in Zhoushan Fishery, to In-fa. Moreover, the possible changes in fishery resources after the typhoon were discussed. This study was conducted to provide support for a future comprehensive assessment of the influence of typhoons on the coastal estuarine ecosystem.

2. Materials and Methods

2.1. Satellite Data

The daily Chl-*a* concentration product was obtained from MODIS-Aqua ocean color remote sensing data (<https://oceancolor.gsfc.nasa.gov/> (accessed on 17 September 2022)). This dataset is a sea surface remote sensing reflectance product that has undergone pre-processing steps, including bow-tie effect removal, geometric correction, and atmospheric correction. For this study, four satellite images taken on 17, 21, 31 July and 8 August 2021, before and after the landing of In-fa, were used. Given that the suspended sediment concentration (SSC) in Hangzhou Bay tended to be higher, reaching up to 1.103 g/L [38], we effectively extracted the Chl-*a* concentration from the area spanning 121°48'E–123°50'E and 29°21'N–31°30'N in order to decrease the impact of SSC on the spatial distribution of Chl-*a* concentration.

The GF-4 satellite, successfully launched on 29 December 2015 [39], operates in geosynchronous earth orbit at an orbital height of 36,000 km. It is equipped with a panchromatic multispectral sensor (PMS) with a resolution of 50 m, mid-wave infrared of 400 m, and width of over 400 m (Table 1). With high temporal and spatial resolution advantages, the satellite has excellent potential and vast space in meteorological weather monitoring, disaster detection, and coastal zone management [40]. This offers quick, dependable, and stable optical remote sensing data for typhoons and other natural disasters. Therefore, we selected four GF-4/PMS L1-level remote sensing images (taken on 20, 21, 31 July and 9 August 2021) from the study area with relatively complete coverage (<https://data.cresda.cn/#/home> (accessed on 16 November 2022)) to perform the inversion of SSC concentration in Zhoushan Fishery.

Table 1. Band information of Gaofen-4 (GF-4) satellite.

Type	Band No.	Spectral Range (μm)	Spatiotemporal Resolution (m)	Width (km)	Revisit Time (s)
Near-Infrared (VINR)	B1 (Pan)	0.45–0.90	50	400	20
	B2 (Blue)	0.45–0.52			
	B3 (Green)	0.52–0.60			
	B4 (Red)	0.63–0.69			
Middle Infrared (MWIR)	B5 (NIR)	0.76–0.90	400		
	B6 (MWIR)	3.5–4.1			

After preprocessing the satellite data using radiometric calibration, atmospheric correction, and orthorectification with ENVI 5.3 software, the changes in SSC concentration in Zhoushan Fishery before and after the typhoon were analyzed using models from previous studies [41]. The equations were as follows:

$$\rho = 314.435 \times B3 + 3805.982 \times B4 + 28.54 \quad (1)$$

where ρ is SSC concentration, and B3 and B4 are divided into green and red band reflectance in the GF-4 image, respectively.

2.2. Reanalysis and Observed Data

Due to the thick cloud cover during typhoons and the relatively frequent fishing activities in the East China Sea, meeting the continuous observation of the response of upper ocean variables after typhoons is challenging [29,35]. In this study, the surface ocean data, including SST, SSS, Chl-*a*, sea-surface wind, and current ocean data, were all obtained from reanalysis products, which provide more comprehensive and systematic spatial and temporal information (Table 2).

Table 2. Data sources and related information.

Field (Units)	Dataset	Data Source	Spatiotemporal Resolution	Recourses
SST (°C)	MUR-SST	NASA JPL PO. DAAC	2 km/1 d	https://registry.opendata.aws/mur (accessed on 29 October 2022).
SSS (psu)	HYCOM GOFS 3.0	HYCOM	0.08°/3 h	https://www.hycom.org/ (accessed on 8 November 2022)
Chl- <i>a</i> (µg/L)	OCEANCOL-OUR_GLO_BGC_L4_MY_009_104	CMEMS	4 km/1 d	https://data.marine.copernicus.eu/ (accessed on 18 November 2022)
10 m <i>u/v</i> components of wind (m/s)	ERA5	ECMWF	0.25°/1 h	https://marine.copernicus.eu/ (accessed on 15 October 2022)
Total precipitation (m/d)	ERA5	ECMWF	0.25°/1 h	https://marine.copernicus.eu/ (accessed on 24 November 2022)
Ocean current (m/s)	HYCOM GOFS 3.0	HYCOM	0.08°/1 h	https://www.hycom.org/ (accessed on 28 November 22)
Topography (m)	ETOPO1	NOAA/NGDC	1 arc-min	http://www.ngdc.noaa.gov/mgg/global/global.html (accessed on 12 September 2022)
Typhoon (lat/lon)	DWRZP	Typhoon track	--	https://typhoon.slt.zj.gov.cn/default.aspx (accessed on 31 August 2022)

MUR-SST: Multi-scale Ultra-high Resolution Sea Surface Temperature; HYCOM: Hybrid Coordinate Ocean Model; GOFS: global ocean forecasting system; OCEANCOLOUR_GLO_BGC_L4_MY_009_104: global ocean colour (Copernicus-GlobColour), biogeochemical, L4 (monthly and interpolated) from satellite observations; NASA: National Aeronautics and Space Administration; JPL: Jet Propulsion Laboratory; PO-DAAC: Physical Oceanography Distributed Active Archive Center; CMEMS: Copernicus Marine Environment Monitoring Service; ECMWF: European Centre for Medium-Range Weather Forecasts; NOAA/NGDC: National Oceanic and Atmospheric Administration/National Geophysical Data Center; DWRZP: Department of Water Resources of Zhejiang Province.

SST was derived from the global, gapless, gridded, daily Multi-scale Ultra-high Resolution Sea Surface Temperature (MUR-SST) dataset provided by the National Aeronautics and Space Administration, with a spatial resolution of up to 2 km. This dataset has a spatial resolution that is orders of magnitude more accurate than the majority of current reanalysis products [42]. The MUR-SST dataset integrates multiple data sources, including satellite, buoy, and ship observations; it is combined with data assimilation techniques to achieve a high-accuracy simulation and prediction of SST. It has been utilized in various fields, such as marine environment monitoring, climate change research, and fisheries resource management, providing valuable information services.

SSS and current data were obtained from the Hybrid Coordinate Ocean Model (HYCOM) ocean circulation model. Unlike the traditional ocean models, HYCOM employs a vertical hybrid coordinate model that combines isopycnic coordinates, vertical *z* coordinates, and terrain-following coordinates. This approach enhances the accuracy of simulation results for global or regional oceans, stratified or non-stratified oceans, oceans, or nearshore areas [43]. With its higher vertical resolution in the surface and shallower coastal regions, the model can represent the physical properties of the nearshore upper ocean well [44,45], which provides reliable data support for the observation of SSS and currents before and after typhoons in the coastal area of Zhoushan Fishery.

The Chl-*a* reanalysis product was derived from global ocean satellite observations at a 4 km spatial resolution as provided by the Copernicus Marine Environment Monitoring Service (CMEMS). This product includes daily and monthly averaged data on global ocean biogeochemical parameters. To assess the suitability of the Chl-*a* reanalysis product within the coastal area of Zhoushan Fishery, we compared it with the surficial in situ Chl-*a* data gathered on 23–24 October 2019 [46] and the CMEMS Chl-*a* data (Figure 1). We calculated the spatial average for the 4 km region surrounding each in situ location. The findings indicated that there was a good correlation between the in situ Chl-*a* and the CMEMS Chl-*a* ($R^2 = 0.625$, RMSE = 0.7662 µg/L), indicating that the CMEMS Chl-*a* was applicable within the coastal area of Zhoushan Fishery.

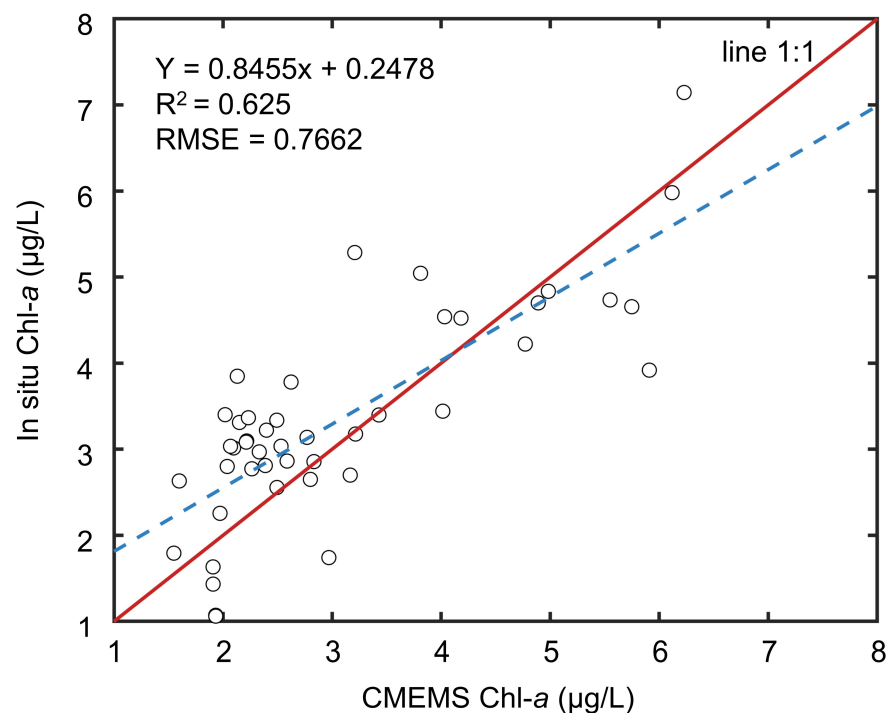


Figure 1. Analysis of the correlation between the in situ and CMEMS Chl-*a* ($\mu\text{g/L}$).

The National Oceanic and Atmospheric Administration (NOAA) (<https://www.ncei.noaa.gov/maps/hourly/>) (accessed on 11 December 2022) provides hourly observations from weather sites around the world and has recorded temperature, pressure, wind direction, wind speed, and rainfall for the period from August 1956 to the present; it was used to obtain the daily average rainfall data before and after the landfall of Typhoon In-fa. This study selected the hourly rainfall data from the Dinghai and Baoying hydrological stations and calculated the daily cumulative rainfall for July 2021.

2.3. Typhoon In-fa and Study Area

The path of Typhoon In-fa is shown in Figure 2. In-fa was generated on 17 July 2021 at 18:00 UTC in the NPO, and it moved westward after it was generated. It intensified into a strong typhoon on the 21st of July at 3:00 UTC, reaching a maximum sustained wind speed of 42 m/s on the 22nd at 0:00 UTC. The minimum surface pressure recorded was 955 hPa, and it exhibited slow movement with a translational speed of 1.4 m/s (Figure 3). It made landfall in the Dinghai District of Zhoushan City, Zhejiang Province, at around 9:00 UTC on 25 July, then moved into Hangzhou Bay on the evening of 25 July, moving northwestward (Figure 2b). Figure 2c displays specific information regarding the study area ($121^{\circ}24'E$ – $123^{\circ}30'E$, $29^{\circ}21'N$ – $31^{\circ}30'N$).

In-fa has the characteristics of strong wind, a slow-moving speed, long influence time, a wide rainfall range, and ample accumulated rainfall. When it made landfall in the coastal area of Zhoushan Fishery (Figure 3), the maximum sustained wind speed was 38 m/s, the minimum surface pressure was 965 hPa, and the translational speed was 2.8 m/s. The duration of rainfall impact was three times the average impact duration of typhoons, with a total precipitation amount of approximately 12.74 billion m^3 , breaking the record for the largest typhoon landfall in Zhejiang Province (China Water Resources Annual Report 2021, <http://www.mwr.gov.cn/>) (accessed on 25 November 2022). This profoundly impacted the marine environment and ecosystem of the estuary and coastal waters.

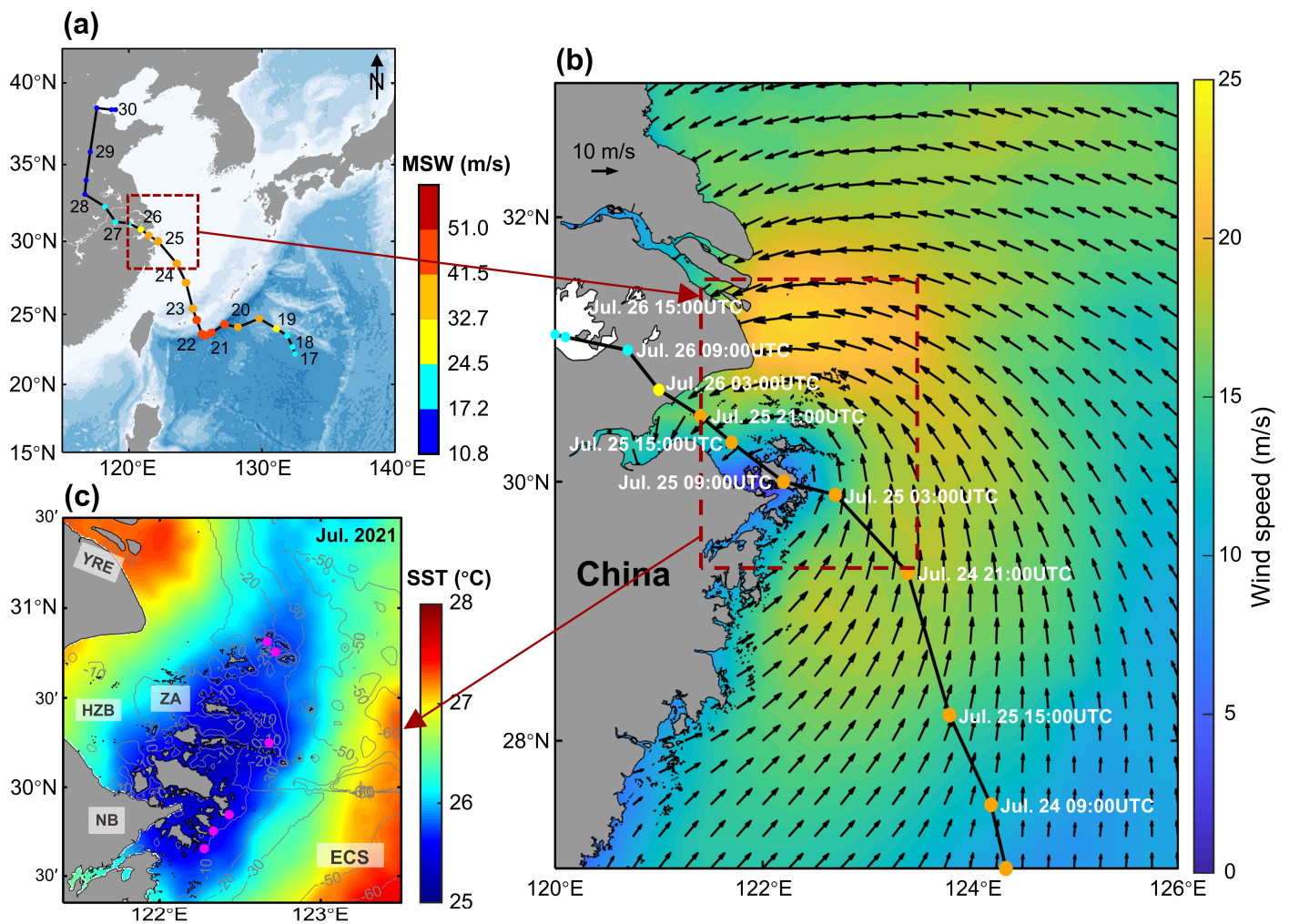


Figure 2. Typhoon In-fa path and study area. (a) The track and intensity of In-fa (MSW: the maximum sustained wind); (b) the wind field vector over East China Sea (ECS) at 09:00 UTC on 21 July 2021, where the color indicates the speed and the black arrow is the wind speed. (c) Sea surface temperature (SST) and its isobath within the research region on July 2021 (the magenta dots: the locations of national marine ranching demonstration areas). YRE: Yangtze River estuary; HZB: Hangzhou Bay; ZA: Zhoushan Archipelago; NB: Ning Bo.

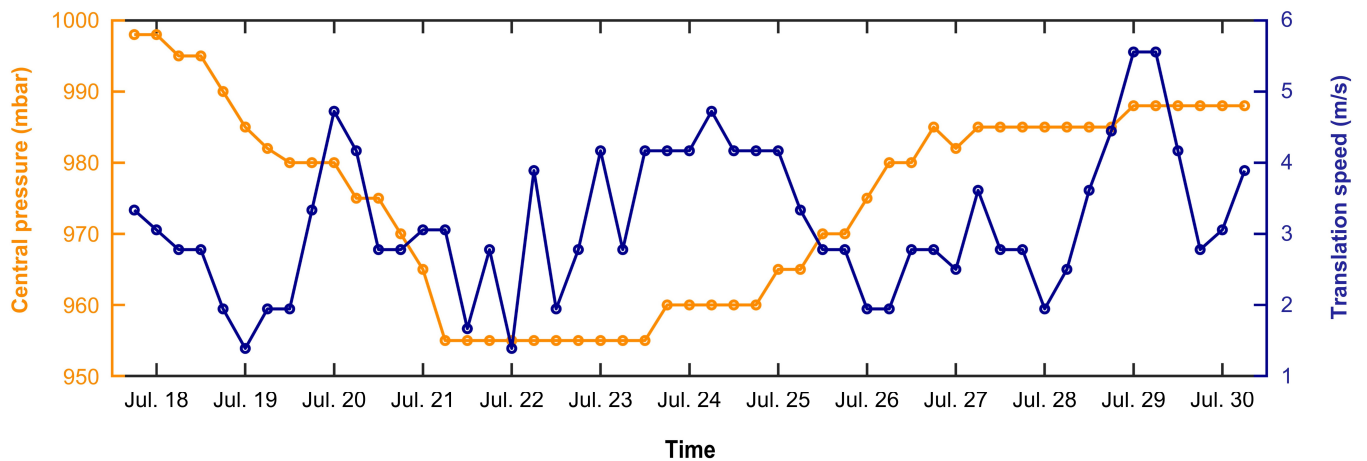


Figure 3. The translational speed and central stress of typhoon In-fa (17–30 July 2021).

2.4. Estimation of Typhoon Impact Factors

To evaluate the possible mechanisms of SST, SSS, and Chl-*a* concentration on In-fa response, we estimated the wind stress power (P_w), Ekman pumping velocity (EPV ; $\times 10^{-5}$ m/s), coastal upwelling velocity, and Ekman current based on the 10 m u/v components of wind data provided by ERA5. The specific calculations for these four factors are as follows.

Wind stress at the sea surface (τ_0) is calculated as:

$$\tau_0 = \rho_{\text{air}} C_D U_{10}^2 \quad (2)$$

where U_{10} represents wind speed at a height of 10 m above mean sea level, as obtained from the ERA5 dataset. ρ_{air} denotes air density (≈ 1.17 kg/m³ at 30 °C), while C_D refers to the drag coefficient.

The P_w value in the upper layer of the ocean is a consequence of the wind-induced kinetic energy flux (W/m²) [31];

$$P_w = \tau_0 U_{10} \quad (3)$$

The EPV is calculated as [47]:

$$EPV = \text{Curl} \left(\frac{\tau_0}{f \times \rho_w} \right) \quad (4)$$

where f denotes the Coriolis parameter, and the value of ρ_w corresponds to the density of seawater, which is 1025 kg/m³.

The surface Ekman current (V_0) is calculated as [48]:

$$V_0 = \frac{0.0127}{\sqrt{|\sin|\varphi|}} U_{10} \quad (5)$$

where φ is the latitude. In the Northern Hemisphere, the surface Ekman current flows at a direction 45° to the right of the wind direction.

The velocity of coastal upwelling (W_C) is calculated as [49];

$$W_C = \frac{\tau_a}{\rho_w f L} \quad (6)$$

where τ_a is the alongshore wind stress and L is the horizontal length scale of upwelling [50]. When W_C is positive, it represents the velocity of the water moving vertically towards the surface due to the upwelling-favorable alongshore wind.

3. Results

3.1. SST Responses before, during, and after In-fa

One of the significant oceanic responses to typhoons is SST [51] (Figure 4). In summer, the nearshore waters of the Zhoushan Islands exhibit an upwelling phenomenon, resulting in SST values that are 0–3 °C lower than the surrounding temperature (Figure 4(a1)). SST within shoreline waters was significantly affected by the landfall of In-fa on 25 July. SST in the research region dropped to about 26 °C with the phenomenon of seawater cooling (Figure 4(a2)), which was about 1–2 °C lower compared with that of before the typhoon (17 July). In addition, the decline in SST in the research region exhibited a distinctive saddle shape, as depicted in Figure 4(b2). Notably, SST obviously decreased on the right side (the sea area northwestern and southeastern of Gouqi Island, bounded by the red triangle), and the decrease was nearly 1–2 °C. Meanwhile, SST in the typhoon center (Zhoushan Islands) experienced a decrease of around 0–1 °C. In contrast, some sea areas in the northeast showed a slight warming indication.

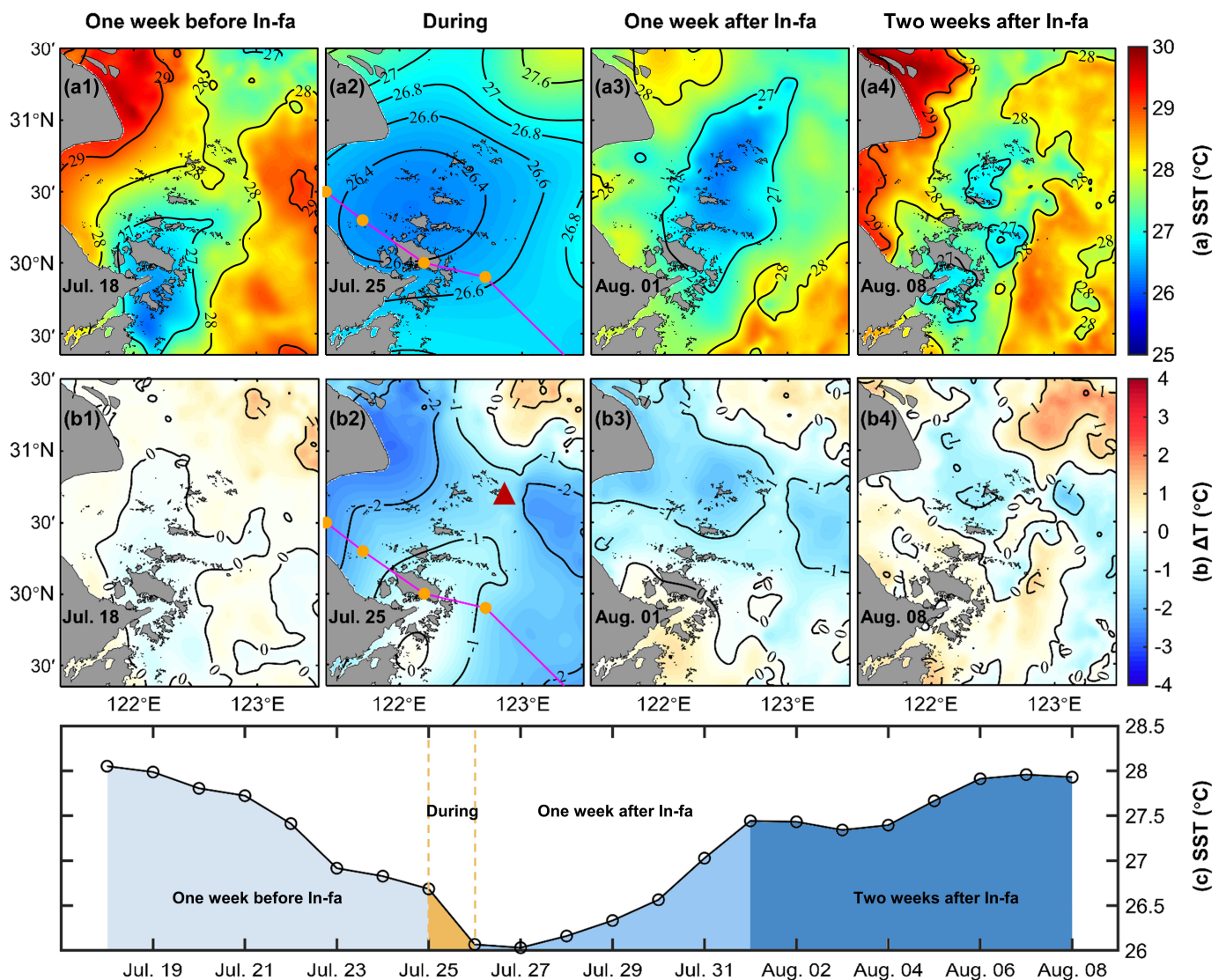


Figure 4. SST distribution before, during, and after the typhoon. (a1–a4): daily average of SST within the research region (b1–b4): Δ SST is a subtraction operation based on the SST of 17 July 2021; (c): time series of SST spatially averaged from 18 July to 8 August 2021. Red triangle: Gouqi Island.

One week after the typhoon (1 August), the SST in the area where the typhoon made landfall began to gradually recover, reaching 27–28 °C. However, low-temperature water persisted in the coastal waters and extended towards the northeast (Figure 4(a3,b3)). Two weeks after the typhoon (8 August), SST in the Yangtze River estuary had mostly returned to its pre-typhoon level, but the low-temperature seawater region had expanded further (Figure 4(a4,b4)).

Based on Figure 4c, the SST continuously decreased from 18 to 27 July as Typhoon In-fa moved northwestward, reaching its lowest value on 27 July with a 2 °C drop. Two weeks after the typhoon, the SST gradually warmed up and returned to its peak on 8 August. Thus, it is evident that the SST in Zhoushan Fishery showed a response to Typhoon In-fa.

3.2. SSS Responses before, during, and after In-fa

Figure 5 illustrates the variation trend of SSS in the research region before and after the period of typhoon transit. In summer, the SSS of the Zhoushan Islands sea area is about 24–33 psu. The SSS isopleth shows a distribution trend of lower western and higher eastern. The sea area to the west of 122°50'E exhibits a more densely distributed salinity gradient, with a flushing freshwater tongue extending eastward in the Yangtze River estuary. In

contrast, the salinity isopleths in the ocean east of $122^{\circ}50'E$ are sparse, and SSS is high (Figure 5(a1)).

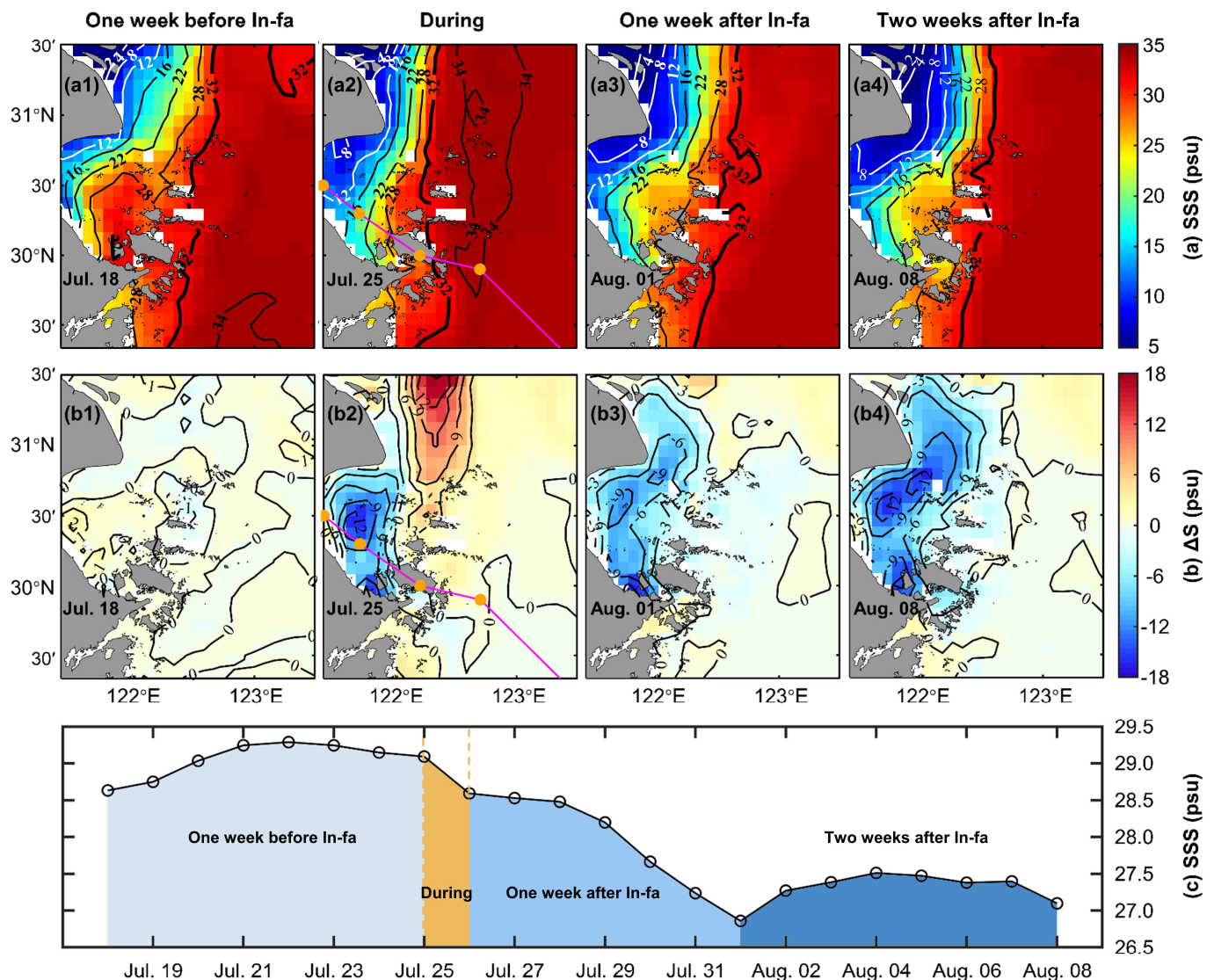


Figure 5. Sea surface salinity (SSS) distribution before, during, and after the typhoon. (a1–a4): daily average of SSS within the research region (b1–b4): Δ SST is a subtraction operation based on the SST of 17 July 2021; (c): time series of SSS spatially averaged from 18 July to 8 August 2021.

The variation in SSS during the landfall of Typhoon In-fa (25 July) differed within the impacted area of the typhoon (Figure 5(a2,b2)). High-salinity seawater advanced westward near the estuary (>32 psu). The SSS (of the Yangtze River estuary) significantly increased by about 0–15 psu (compared with the salinity value on 17 July), while the salinity in the sea around the typhoon center (the Hangzhou Bay estuary) decreased by 0–12 psu. During the two weeks following the typhoon (1 and 8 August) (Figure 5(a3,a4,b3,b4)), SSS at the inlet exhibited more noticeable changes, and the low-salinity seawater continued to spread northeastward, becoming more widely distributed. SSS at the Yangtze River Estuary ($121^{\circ}24'E$ – $122^{\circ}40'E$, $30^{\circ}45'N$ – $31^{\circ}30'N$) transitioned from an increasing trend to a decreasing trend, decreasing by about 0–9 psu.

According to Figure 5c, the average daily SSS within the research region exhibited an overall increasing trend during the week preceding the typhoon (18–24 July). However, after the typhoon made landfall (25 July–1 August), SSS began to decline from 29.09 to 26.86 psu (down 7.6%). Two weeks after the typhoon's landfall (2–8 August), SSS re-

bounded, but it remained approximately 1–2 psu lower than the pre-typhoon SSS peak. These results suggest that typhoons have a delayed and persistent impact on SSS within the research region. To further understand the factors contributing to the distribution of SSS variations, the combined effects of changes in vertical mixing, rainfall, and currents on SSS will be analyzed in Section 4.1.2.

3.3. Chl-*a* Responses before, during, and after In-fa

During Typhoon In-fa, the Chl-*a* data may be significantly affected by cloud cover occlusion and the limited observation frequency of MODIS products. The reanalysis data can effectively supplement the missing data. Therefore, it is necessary to combine MODIS satellite data (Figure 6a) and CMEMS reanalysis data (Figure 6b) for a comprehensive observation of surface Chl-*a* concentration pre- and post-typhoon. Because the typhoon significantly altered the spatial distribution of Chl-*a* concentration within the research region, a differential analysis of Chl-*a* concentration was not performed in this section.

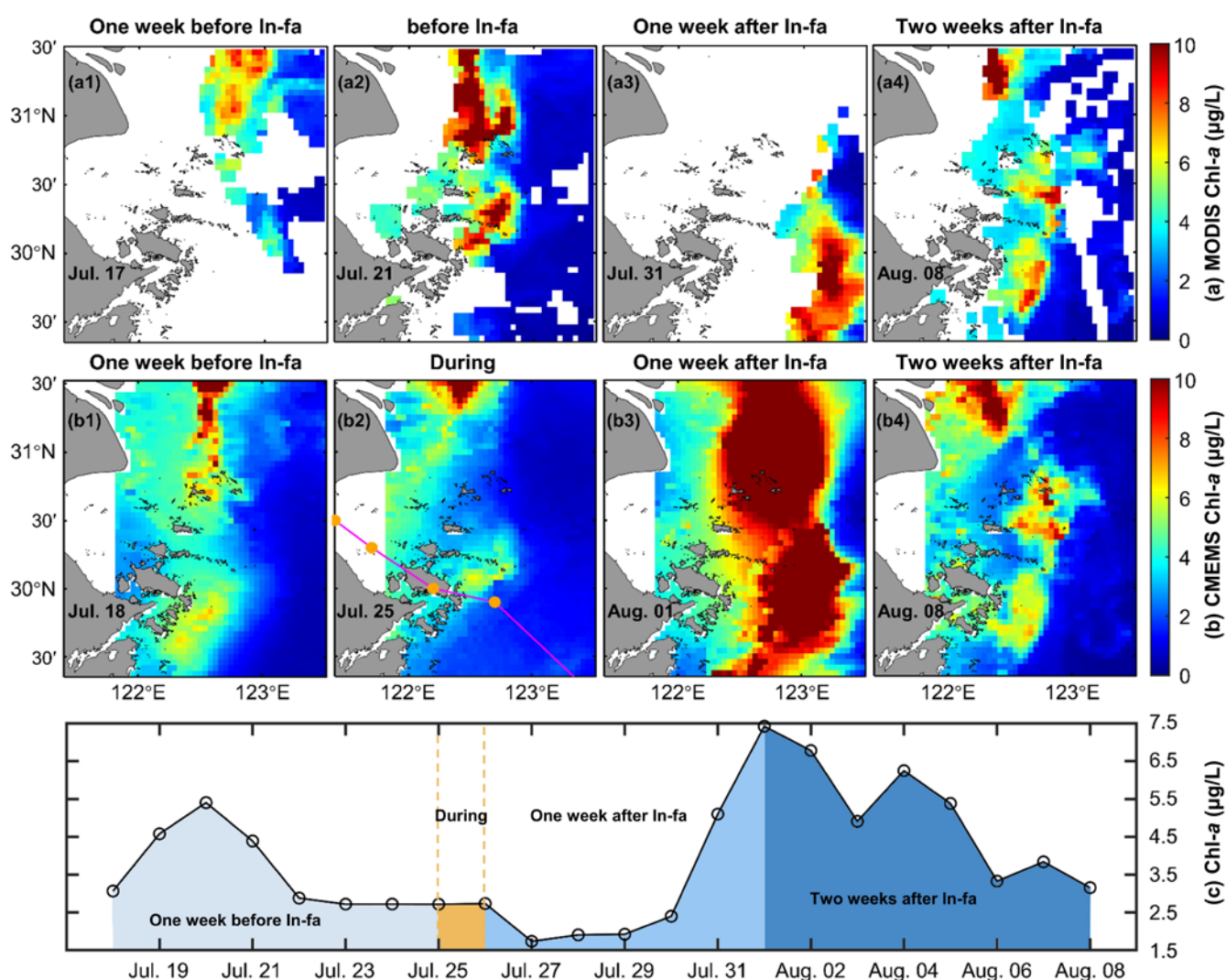


Figure 6. The change in sea surface Chl-*a* concentration before, during, and after the typhoon. (a1–a4,b1–b4): the daily average of Chl-*a* (c): time series of Chl-*a* concentration in terms of spatial means from 18 July to 8 August 2021.

During the pre-typhoon period (17 and 18 July), higher Chl-*a* concentration values of approximately 3–9 $\mu\text{g/L}$ were observed in the island-dense areas of Zhoushan Islands, particularly in the waters west of 123°E (Figure 6(a1,a2,b1)). Chl-*a* concentration in the

east of longitude 123°E was low, around 0.5–3 µg/L. During the landfall of the typhoon (25 July), waters with high Chl-*a* shifted towards the west. The concentration of Chl-*a* in the island-dense waters significantly decreased to about 1–4 µg/L. Meanwhile, the concentration of Chl-*a* in Hangzhou Bay and the Yangtze River estuary remained high, at approximately 3–9 µg/L (Figure 6(b2)).

One week after the typhoon (31 July and 2 August), there was a significant increase in Chl-*a* concentration within the research region, as shown in Figure 6(a3,b3). The waters with high Chl-*a* concentration shifted eastward, spanning from 123°E to 123°30'E, with concentrations ranging from about 5 to 10 µg/L. Large-scale phytoplankton blooms were observed within the research region. Two weeks after the typhoon (8 August) (Figure 6(a4,b4)), the spatial distribution of Chl-*a* concentration within the research region generally remained the same as before the typhoon.

The average daily Chl-*a* (Figure 6c) exhibited a decrease from 5.40 to 2.72 µg/L (49.7% decrease) in the four days before the typhoon's passage (21–24 July). Two days after the typhoon (27 July), it reached the lowest value of about 1.74 µg/L, followed by a continuous increase in Chl-*a* during the first week after the typhoon, reaching a maximum value of 7.42 µg/L on 1 August. This indicates that typhoons not only promote the flourishing of Chl-*a* but also have delayed effects, which is consistent with previous studies [52]. By two weeks after the typhoon (1–8 August), the Chl-*a* concentration had generally returned to the pre-typhoon level.

4. Discussion

4.1. The Contribution of the Typhoon to the Change in Typical Environmental Factors

To investigate the response mechanisms of typical oceanic environmental factors (SST, SSS, and Chl-*a*) to In-fa, we estimated the P_w , EPV, coastal upwelling velocity, and sea surface Ekman current using Equations (3)–(6). Additionally, we examined variations in sea surface currents, rainfall, and SSC concentration within the research region before and after In-fa to gain a comprehensive understanding of these mechanisms.

4.1.1. The Mechanism of Typhoon Effect on SST

Typhoons can cause significant disturbances in the upper ocean when they pass over it. One notable change in the upper ocean within the research region during the arrival of Typhoon In-fa was the cooling of the sea surface, especially on the right side of the typhoon (Figure 4). This response is related to the vertical mixing caused by the typhoon and the temperature structure in the vertical direction before the storm [7,53].

During the typhoon's landfall, the EPV within the research region was significantly enhanced (Figure 7a). This intense Ekman pumping resulted in the intensification of vertical seawater mixing. Furthermore, the relatively shallow water depth near the Zhoushan Islands (5–60 m) (Figure 2c) led to a rapid increase in upwelling velocity, which reached 0.957×10^{-4} m/s (Figure 7b). It has been observed that the coastal area of Zhoushan Fishery experiences significant thermal stratification during the summer, with a temperature difference of around 1–8 °C between the surface and bottom waters [54]. As a result of the strong vertical exchange and mixing between the cold bottom water and surface water, along with the increased net heat flow [55], the SST in the study area notably decreased by about 2 °C (Figure 4(a2)).

After the typhoon landed, there was a significant increase in upwelling strength within the research region, although the distribution of upwelling energy across space was uneven. The spatial distribution of P_w and EPV along the In-fa track (Figure 8) revealed that the intense P_w impacted the ocean surrounding the typhoon track except for its center. Notably, the right side of the typhoon track exhibited a particularly strong P_w (Figure 8a). Meanwhile, the physical values of EPV (red for upwelling, blue for downwelling) (Figure 8b) indicated that the vertical water exchange occurred along the center of the typhoon track, with the majority of the upwelling energy being centered on the right side of the typhoon (Figure 8(b3–b6)). The above phenomenon resulted in a stronger current response on the

right side of the typhoon track within the research region, leading to increased mixing and a more pronounced weakening of SST (Figure 4(b2)). It is worth noting that the decrease in SST and strength of the Ekman effect are well-correlated [56–58].

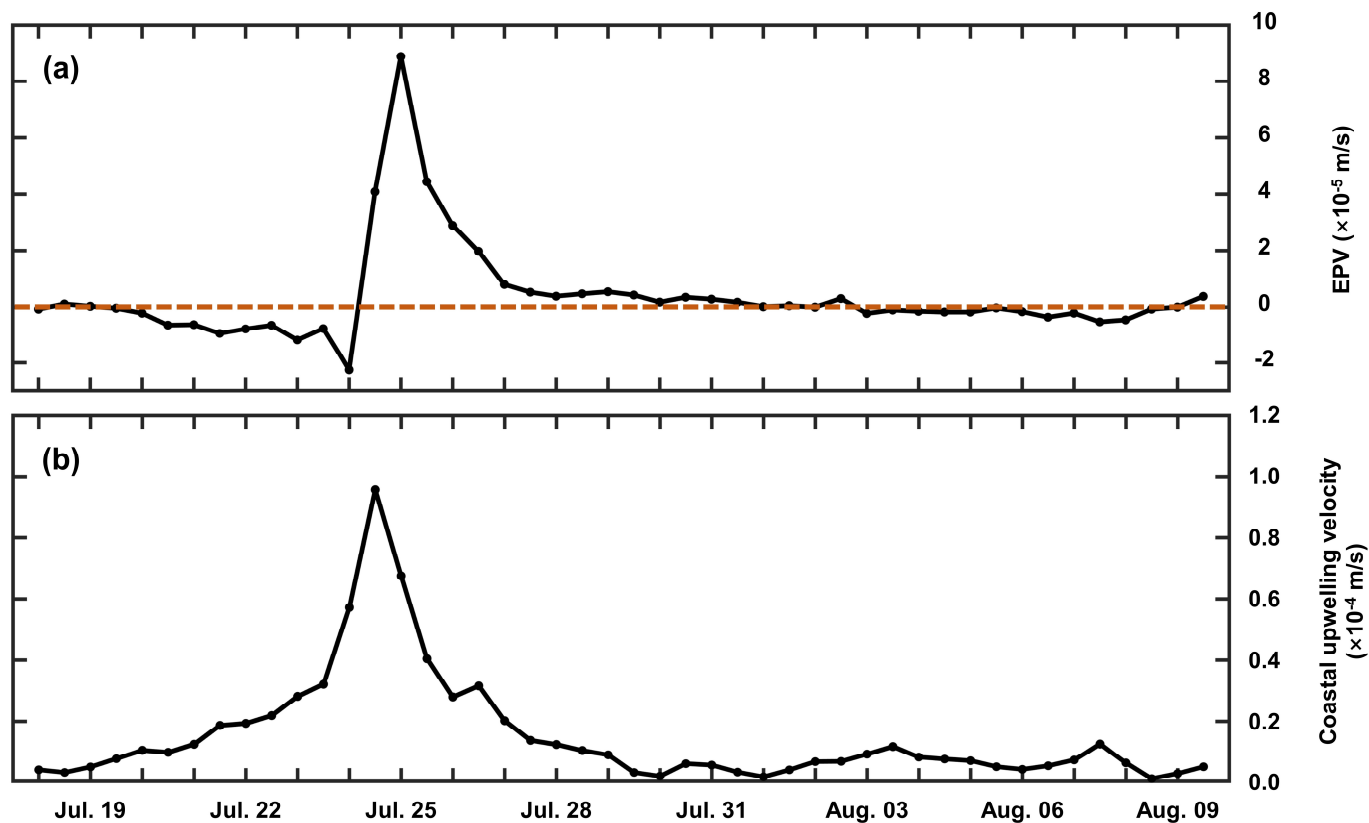


Figure 7. The average Ekman pumping velocity (*EPV*, positive upward) and coastal upwelling velocity in the coastal area of Zhoushan Fishery during the typhoon. (a): The average Ekman pumping velocity (b): coastal upwelling velocity.

Moreover, the variability in the spatial distribution of SST cooling is influenced by the pre-typhoon temperature structure in the vertical direction of the sea. SST cooling is typically observed in regions with a shallow mixed layer and steep vertical temperature gradient [6,58]. Prior to the typhoon's arrival, the coastal area of Zhejiang experienced an upwelling phenomenon in the sea surrounding the Zhoushan Islands due to the influence of the southwest monsoon and topography [59]. This resulted in a 1–3 °C reduction of sea surface temperature compared with neighboring regions (Figure 4(a1)). Moreover, the upwelling-affected area exhibited a smaller vertical gradient of temperature and deeper mixed layer depth compared with the Yangtze River estuary [54], contributing to the more prominent cooling of SST in the latter region (Figure 4(b2)).

During the passage of Typhoon In-fa, intense spiral updrafts were generated at the center of the typhoon. As the airflow reached a certain height and diverged, it mixed with the surrounding air and then sunk to the lower levels, often leading to the formation of high-temperature weather in the periphery of the typhoon. The study found signs of SST warming on the northeast side of the research region (Figure 4(b2)), which were related to the reduced upwelling effect due to the downwelling of seawater in the region during the landfall of In-fa (Figure 8(b4)), as well as the high-temperature climatic conditions.

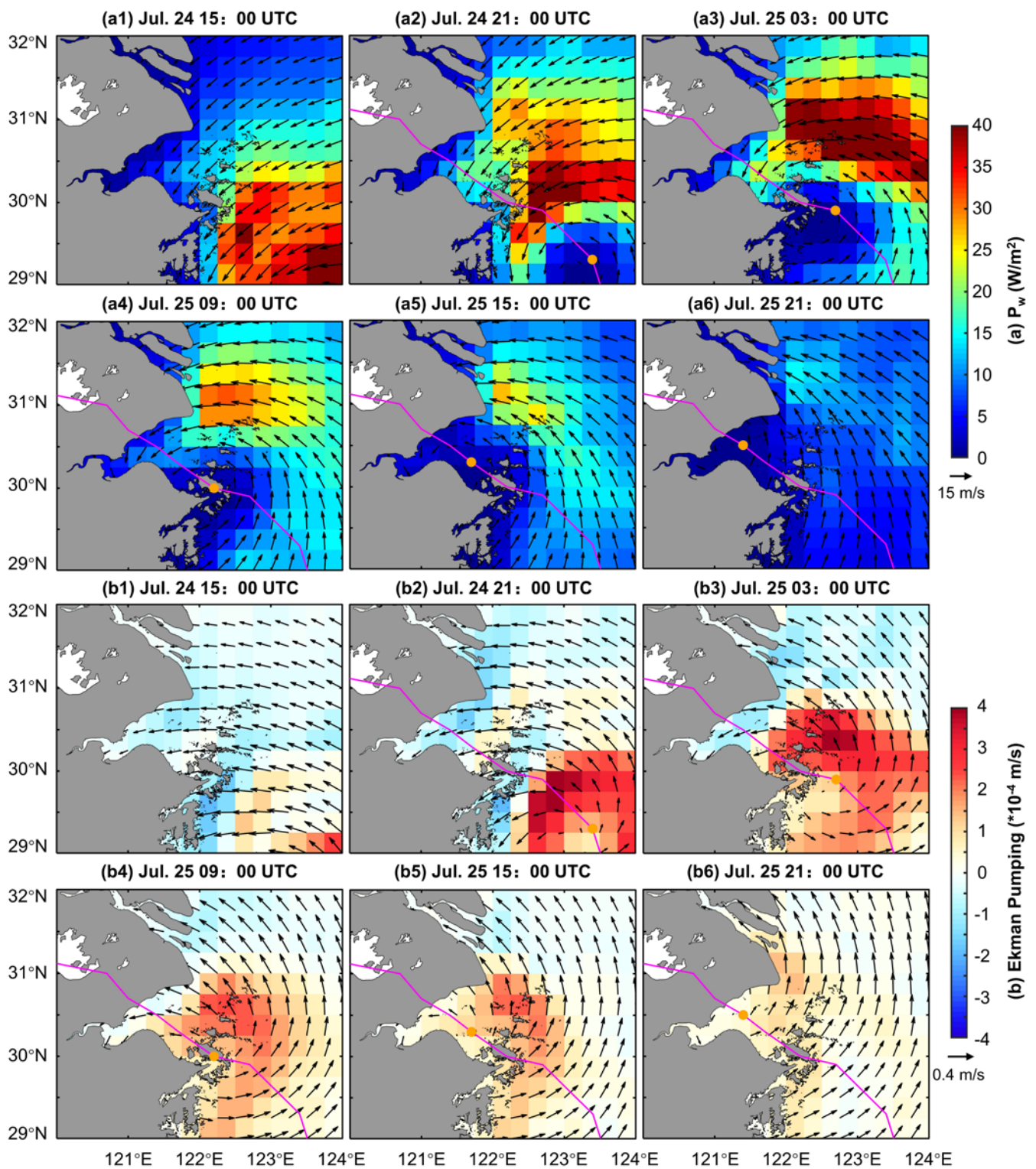


Figure 8. Spatial distribution of wind stress power (P_w) and EPV. **(a1–a6):** P_w and sea surface wind (arrows represent wind speeds and directions). **(b1–b6):** EPV and sea surface Ekman current (arrows represent current speeds and directions); the track of the typhoon and its intensity (magenta line; orange dots).

4.1.2. The Mechanism of Typhoon Effect on SSS

After Typhoon In-fa passed through, the SSS of the study area showed a decreasing trend and was spatially varied (Figure 5), which was related to the changes in the vertical mixing of seawater, rainfall, and sea surface currents brought about by the typhoon [32].

The coastal area of Zhoushan Fishery is located at the confluence of highly saline offshore waters and coastal waters, and the salinity of seawater is particularly stratified in summer [53]. The TWC, YDW, and ZMCC converging currents in the study area were deflected parallel northward and eastward before In-fa landfall. However, the surface currents were enhanced and significantly shifted after In-fa's landfall (Figure 9). Some of the TWC tributaries flowed into the northern part of the Zhoushan Islands and then into the Yangtze River estuary (Figure 9b), which resulted in the influx of high-salinity outer seawater towards the nearshore of the Yangtze River estuary (Figure 5(a2)). Meanwhile, the stronger P_w and EPV on the right side of the typhoon track (Figure 8) induced intense vertical mixing, resulting in high-salinity bottom water being brought to the sea surface. This increased SSS at the Yangtze River Estuary (Figure 5(b2)).

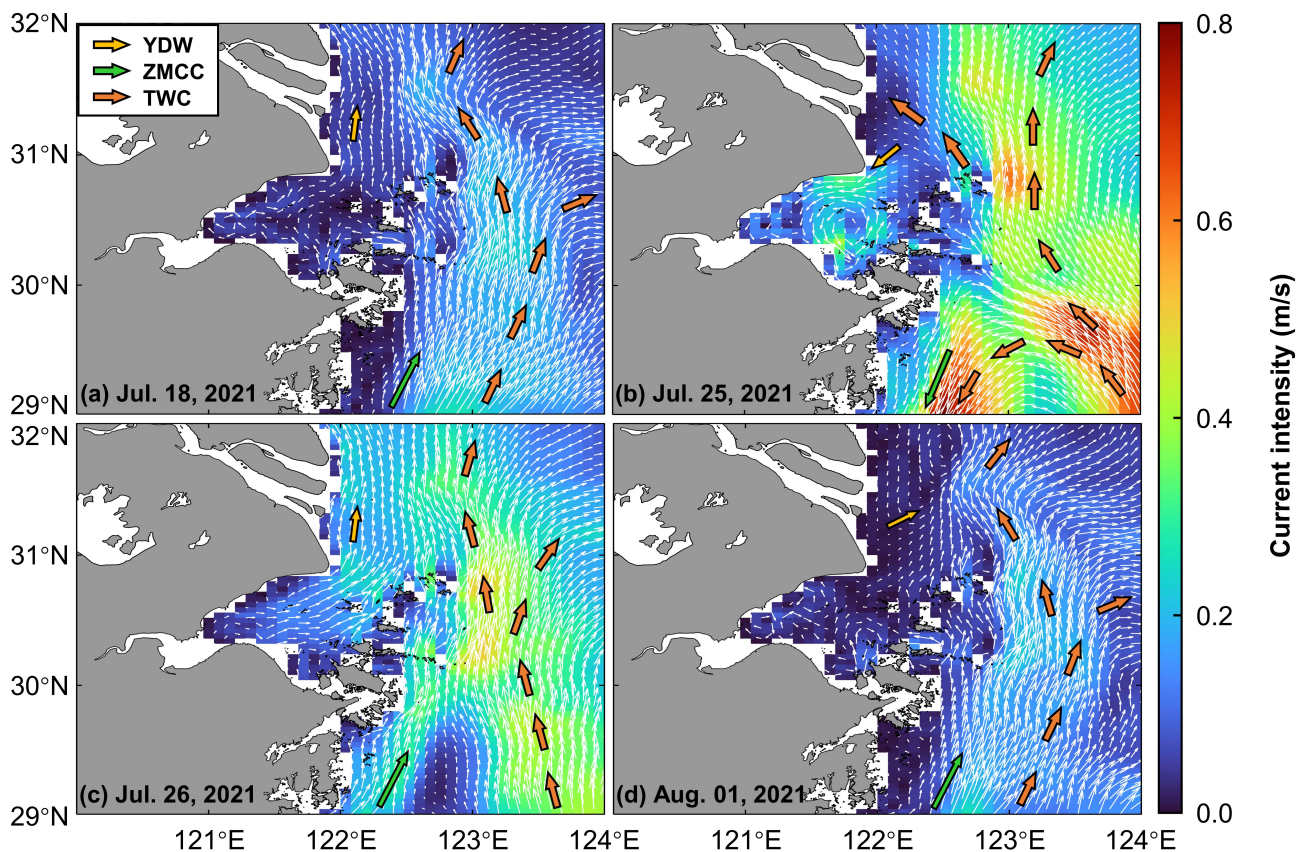


Figure 9. Sea surface currents distribution before, during, and after the typhoon. YDW: Yangtze diluted water; ZMCC: Zhemín coastal current; TWC: Taiwan warm current.

The study found that rainfall occurred two days before In-fa landfall in the waters of Zhoushan Islands (Figure 10(a1,a2)). On 24 July, the average daily rainfall exceeded 200 mm/d (Figure 10b). As In-fa transited, intense rainfall covered the entire Yangtze River estuary and Hangzhou Bay area (Figure 10(a3,a4)). On 26 July, the rainfall was as high as 355 mm/d, which was approximately five times the rainfall before In-fa made landfall (Figure 10b).

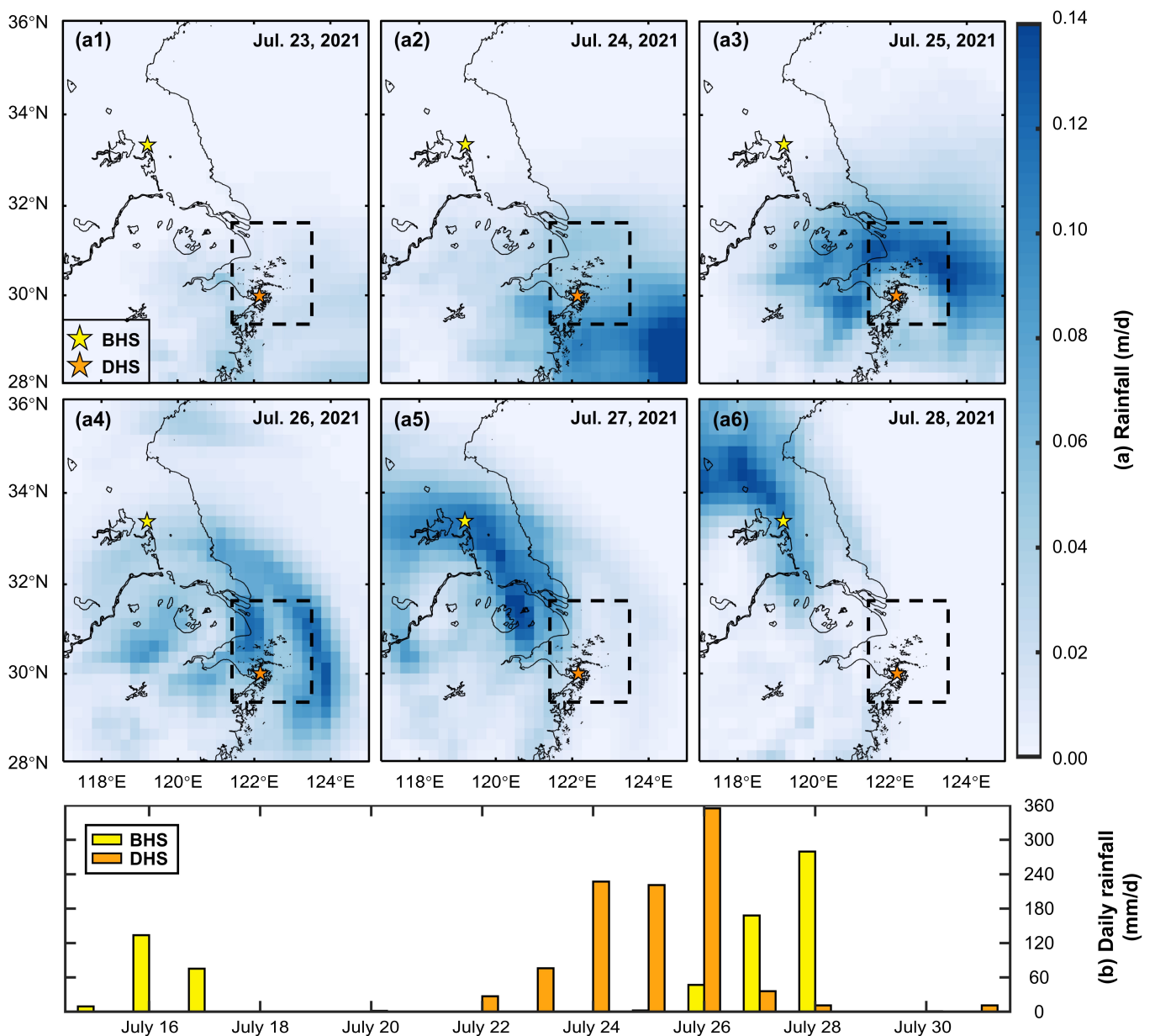


Figure 10. Spatial distribution and daily variation of rainfall within the research region before and after the passage of In-fa. (a1–a6): Spatial distribution of rainfall; (b): daily rainfall at hydrological stations from 15 to 31 July 2021. DHS: Dinghai hydrographic station; BHS: Baoying hydrographic station; black box: study area.

Furthermore, the typhoon's strong winds caused the ZMCC to deflect to the southwest, reducing the inflow of high-salinity seawater into the Hangzhou Bay from nearshore, while the YDW flushed into the bay in the southwest direction (Figure 9b). Under the combined effect of these factors, SSS in Hangzhou Bay rapidly decreased (Figure 5(b2)). The integrated impact of intense Ekman and vortex upwelling at this time had little impact on SSS in the center of the typhoon track compared with intense rainfall [60].

Although the rainfall in the research region decreased after the transit of In-fa, rainstorms continued to erode the runoff in the upper reaches of the Hangzhou Bay and the Yangtze River estuary (Figure 10(a5,a6,b)), which resulted in a surge in runoff volume and floods in multiple locations. This increased the possibility of a massive influx of diluted water into the coastal estuary after the typhoon. Meanwhile, lower salinity seawater from Hangzhou Bay flowed into the Yangtze River estuary in the northeast (Figure 9c,d). As

a result, the SSS in the Yangtze River estuary changed from an increase to a decrease after the typhoon, and the lower salinity seawater continued to spread to the northeast (Figure 5(a3,a4,b3,b4)).

In-fa induced Ekman pumping significantly contributed to the rise in SSS, while rainstorms and changes in currents efficiently decreased SSS; this is a phenomenon that has also been observed in other nearshore seas [33,58,61].

4.1.3. The Mechanism of Typhoon Effect on Chl-*a*

Previous studies [46,62,63] have shown that Chl-*a* concentrations are higher in the coastal area of Zhoushan Fishery in summer (Figure 6(a1,a2)), which is probably due to the rich nutrients carried by the Yangtze diluted water, coastal upwelling, and sufficient sunlight. The maximum Chl-*a* concentration usually occurs at the surface or subsurface layers, and the concentration decreases with depth [62].

Chl-*a* concentrations in the coastal area of Zhoushan Fishery exhibited a relatively swift response to the typhoon (Figure 6). In the four days leading up to the typhoon's landfall (20–24 July), the study area experienced downwelling (negative *EPV* values indicate the presence of wind-induced downwelling) (Figure 7a). This downwelling caused the transport of nutrients rich in surface seawater to the bottom layer, and the nutrients required for phytoplankton growth were not immediately replenished. Consequently, there was a rapid decline in Chl-*a* concentration in the upper layer of coastal seawater (Figure 6c).

Chl-*a* concentrations within the research region decreased during the five days after the typhoon (Figure 6c), and this phenomenon has also been reported in other coastal waters [12,48,64]. On the one hand, the seawater with high salinity and low Chl-*a* concentration continued to invade the nearshore under the northwestward currents (Figures 6(a2) and 9b). On the other hand, the high cloudiness during the typhoon impact could not provide sufficient light for good phytoplankton growth, which limited the growth of Chl-*a* concentration to some extent [65].

The study found that the SSC concentration corresponded well with the high and low Chl-*a* concentration during the week before and after the typhoon (Figure 11(a1,a2,a3,b1,b2,b3)). Before Typhoon In-fa, the estuary (the sea west of 121°48'E) exhibited a high suspended matter concentration. Subsequently, the scouring effect of In-fa, combined with rainstorms in mountainous and river entrances, as well as the vertical mixing of seawater, resulted in an increased SSC concentration in nearshore waters after the rainstorm, which then spread to the outer sea (Figure 11(b3)). This process caused a large influx of nutrients from land-based sources into the coastal waters, while upwelling caused nutrient resuspension [12], creating favorable conditions for phytoplankton blooms in the week after the typhoon (Figure 6(a3,b3)).

Moreover, the lag time in nutrient uptake by phytoplankton growth (average turnaround time of 2–7 days) [52], combined with the transport of offshore currents (Figure 9d), contributed to extensive phytoplankton blooms and the peak Chl-*a* concentration as of the seventh day following typhoon landfall (Figure 6(b3,c)).

After the passage of a typhoon, seawater was stable regarding vertical mixing and upwelling. During a certain period, the nutrient concentration on the sea surface presented a comparatively steady state and could not promote unlimited chlorophyll growth [66]. In addition, the high concentration of SSC continues to persist in nearshore waters following typhoons, leading to a decrease in seawater transparency (Figure 11(b4)), while insufficient light can also limit the growth of phytoplankton in high-turbidity areas [67]. Therefore, during the second week after typhoon landfall, Chl-*a* concentration gradually decreased and returned to pre-typhoon landfall levels (Figure 6(a4,b4)).

In summary, the intense rainfall brought about by In-fa, the upwelling of low-temperature and high-salt bottom water resulting from enhanced vertical mixing, and the influx of diluted water have collectively contributed to an overall decrease in SST and SSS after the typhoon's transit. Meanwhile, this mixing and transport of land-based substances have introduced abundant nutrients to the surface layer of the sea, promoting the growth of

phytoplankton. Consequently, Chl-*a* concentration increased and peaked a week after the typhoon's landfall.

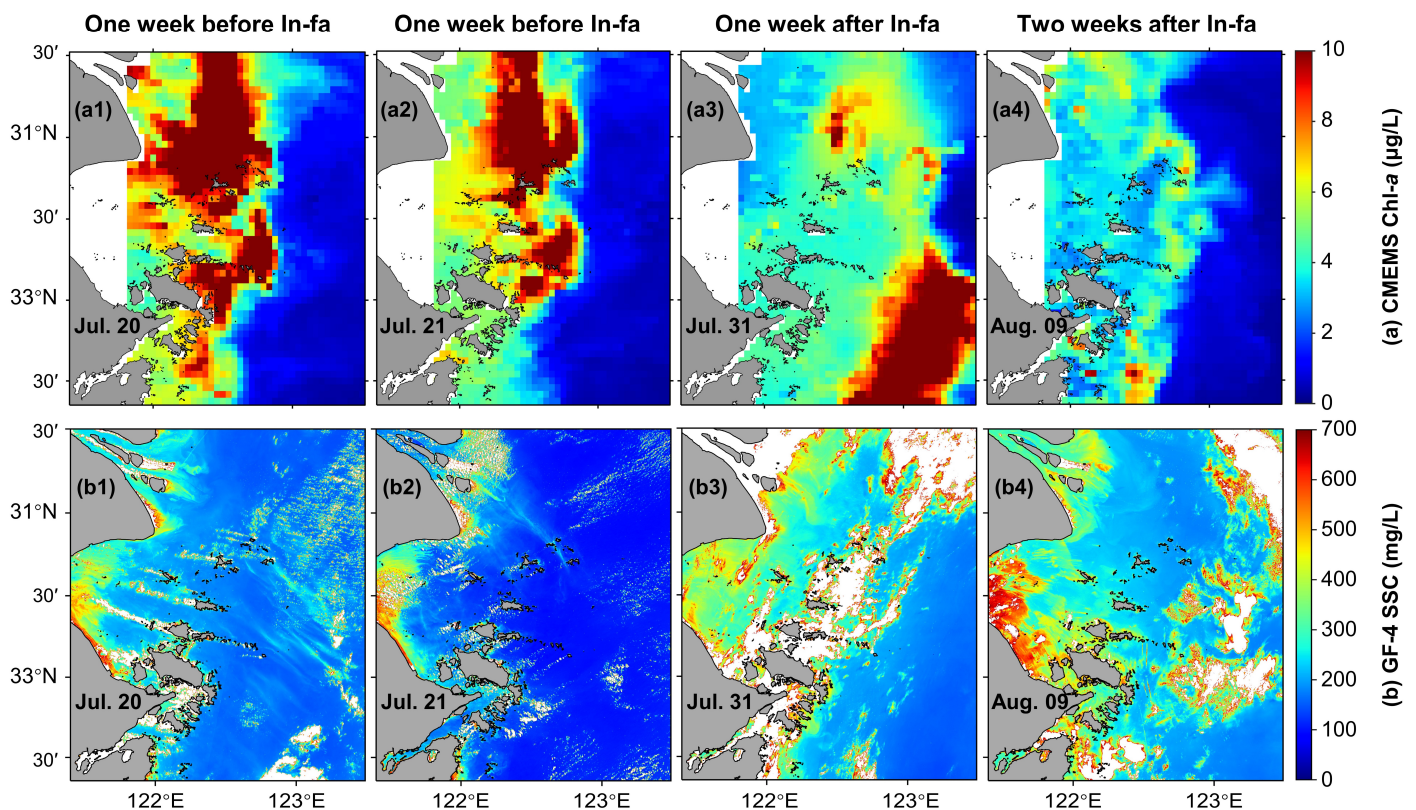


Figure 11. Variations in SSC and Chl-*a* concentration before and after the passage of In-fa. (a1–a4): Spatial distribution of the CMEMS Chl-*a* concentration; (b1–b4): spatial distribution of the SSC concentration.

4.2. The Contribution of Typhoon to Fishery Resources

The strong winds, decreased salinity, increased runoff, increased intensity of currents, upwelling phenomena, and local phytoplankton bloom production brought about by typhoons usually result in positive or negative changes in local fish behavior and community composition [17,24,68]. Summer is a crucial period for breeding the main economic fish and for the growth of juvenile fish in Zhoushan Fishery; at the same time, the landing of Typhoon In-fa directly or indirectly affects the biological processes in the six national marine ranching demonstration areas around the Zhoushan Islands.

Previous studies have shown a strong correlation between changes in the biomass density of fish eggs and larvae and variations in Chl-*a* concentration in the water [46], indicating that Chl-*a* is a reliable indicator of phytoplankton biomass and the prior status of the aquatic food chain [69]. Additionally, Chl-*a* levels can influence the fertility of waters and help evaluate the potential productivity of fishing grounds [70,71]. Chl-*a* concentrations at the sea surface within the research region were significantly increased and more widely distributed by In-fa (Figure 6(b3)). This was closely related to the sizeable terrestrial nutrient discharge in the estuary after the typhoon [13] and the enhanced upwelling effect [17], which increased nutrients. Fish actively migrate through feeding activities to nutrient-rich waters [17,18,72], making it an excellent place to catch fish. The increase in nutrient salinity after typhoons induces an enhancement in Chl-*a* concentration, which has a steady positive effect on fish.

Currents play an essential role in fish productivity [20,73]. The surface currents within the research region were significantly enhanced by In-fa (Figure 9b,c), and some weakfish will enter the nearshore waters due to strong currents [17]. In the week after the typhoon, the TWC formed some small flow sets, cyclones, and anticyclonic eddies in the waters

near the Zhoushan Islands during its northward movement. The sea had upwelling and downwelling currents (Figure 9d). This process allows for sufficient seawater exchange, creates an ideal environment for nutrient salt operation, and creates different current conditions for fish selection, which positively impacts the increase in fishery resources [74,75]. In addition, typhoons lead to violent disturbances of seawater, which will scatter the density of fish and cause them to flee to calmer deep water or the leeward side of the island with less wind and waves, which is an excellent place to catch fish [76].

Species that can quickly adapt to environmental changes can survive in the original waters or enter the changing waters and vice versa, and they will flee from the original survival waters [17]. Several studies have indicated that small- and medium-sized nearshore fish dominate the record of increases after typhoons, while the proportion of small fish at relatively low trophic levels decreases [17,77]. The salinity and temperature in the fishery dramatically changed after the landing of In-fa (Figures 4 and 5). Rainstorms brought about by In-fa decreased SSS in the culture area, which cause fish that are adapted to higher-salinity to swim to higher-salinity waters offshore. In contrast, the freshwater fish population has increased [78]. The decrease in SST will reduce the number of fish that prefer a warm water environment, while the cool water-loving fish living at the bottom will swim to the sub-surface layer where the temperature decreases [77]. In addition, the strong vertical mixing of seawater caused by typhoons can weaken or eliminate the thermocline, causing fish to disperse and be challenging to catch. Lower pressure will cause bottom-dwelling fish to float, which affects bottom trawl production [76].

In summary, the mechanisms underlying fish resource changes in nearshore fisheries after typhoons are complex and can be influenced by various environmental factors, including temperature, salinity, Chl-*a*, and currents. Different species of fish have different degrees of adaptation to these environmental factors. This information helps fishermen obtain a better grasp of the relationship pattern between typhoons and fishing, provides a reference for the distribution of fish stocks, and predicts the direction of fishery movement.

5. Conclusions

Grounded in Zhoushan Fishery, this study used GF-4, MODIS satellite, and reanalysis data to investigate the responses of environmental factors, including SST, SSS, and Chl-*a*, in Zhoushan Fishery around the landfall of Typhoon In-fa, where we analyzed the mechanism.

Typhoon In-fa induced SST, SSS, and Chl-*a* changes. After the landing of In-fa, the intense vertical mixing and enhanced upwelling caused SST to decrease by about 2 °C. In the Northern Hemisphere, the asymmetrical typhoon wind pressure and vertical differences in the temperature structure in front of the typhoon (mixed layer depth and vertical temperature gradient) led to a more intense cooling of SST in the right In-fa track. SST returned to its pre-typhoon peak after two weeks. SSS decreased overall after In-fa landing, and the variation in SSS was spatially variable. SSS was significantly lower in Hangzhou Bay at the eye of the typhoon due to heavy rainfall and runoff; in comparison, the SSS was significantly higher at the Yangtze River estuary on the right side of the typhoon track, which is attributed to the strong *EPV*. MODIS satellite and reanalysis data revealed that the change process of Chl-*a* concentration at the sea surface manifested in a decrease and then an increase. On the seventh day following the typhoon, large-scale phytoplankton blooms appeared, and Chl-*a* concentration was higher than pre-typhoon levels. The spatial and temporal variation in Chl-*a* concentration was intimately correlated with the changes in light intensity, nutrients, current, and SSC after In-fa.

Furthermore, the alterations of physical and biotic variables within the fishery caused by In-fa can affect fishery fish behavior and community composition. The mechanisms of fish resource changes in the nearshore fishery after typhoons are complex and can lead to changes in temperature, salinity, Chl-*a*, and currents, among other environmental factors. This study provides some reference to reveal the response of environmental factors to typhoons and their effects on fishery resources in the fishery with intensive islands in nearshore estuarine shallow waters.

Author Contributions: Conceptualization, R.T. and L.C.; methodology, L.C.; software, R.T.; validation, R.T. and L.C.; formal analysis, R.T., L.C. and X.Y. (Xiaomin Ye); investigation, R.T., L.C., X.Y. (Xiaojun Yan), X.Y. (Xiaomin Ye), Y.X. and J.Y.; data curation, R.T. and L.C.; writing—review and editing, R.T.; writing—review and editing, L.C. and X.Y. (Xiaojun Yan); visualization, R.T.; supervision, L.C.; project administration, L.C.; funding acquisition, L.C. All authors have read and agreed to the published version of the manuscript.

Funding: This work was supported by the following research projects: the Science Foundation of Donghai Laboratory (DH-2022KF01010); the National Natural Science Foundation of China Key international (regional) cooperative research project (42020104009); and the Basic Public Welfare Research Program of Zhejiang Province (LGF21D010004).

Data Availability Statement: Publicly available datasets were analyzed in this study. GF-4/PMS satellite data are available at <https://data.cresda.cn/#/home> (accessed on 7 November 2022).

Acknowledgments: The authors would like to thank the China Centre for Resources Satellite Data and Application for providing the GF-4/PMS satellite data free of charge.

Conflicts of Interest: The authors declare no conflict of interest.

References

- Chan, J.C.L. Interannual and interdecadal variations of tropical cyclone activity over the western North Pacific. *Meteorol. Atmos. Phys.* **2005**, *89*, 143–152. [[CrossRef](#)]
- Ding, P.; Hu, K.; Kong, Y.; Hu, D. Numerical Simulation of Storm-induced Erosion/Deposition in Yangtze Estuary—A Case Study of Typhoon Jelawat. *J. Sediment Res.* **2003**, *6*, 18–24. [[CrossRef](#)]
- Guo, J.; Zhang, T.; Xu, C.; Xie, Q. Upper ocean response to typhoon Kujira (2015) in the South China Sea by multiple means of observation. *J. Oceanol. Limnol.* **2019**, *38*, 314–333. [[CrossRef](#)]
- Pudov, V.D.; Petrichenko, S.A. Trail of a typhoon in the salinity field of the ocean upper layer. *Izv. Atmos. Ocean Phys.* **2000**, *36*, 645–650.
- Price, J.F. Upper Ocean Response to a Hurricane. *J. Phys. Oceanogr.* **1981**, *11*, 153–175. [[CrossRef](#)]
- Price, J.F.; Morzel, J.; Niiler, P.P. Warming of SST in the cool wake of a moving hurricane. *J. Geophys. Res. Ocean.* **2008**, *113*, C07010. [[CrossRef](#)]
- Chiang, T.L.; Wu, C.R.; Oey, L.Y. Typhoon Kai-Tak: An Ocean’s Perfect Storm. *J. Phys. Oceanogr.* **2011**, *41*, 221–233. [[CrossRef](#)]
- Jiang, X.; Zhong, Z.; Liu, C. The effect of typhoon-induced SST cooling on typhoon intensity: The case of Typhoon Chanchu (2006). *Adv. Atmos. Sci.* **2008**, *25*, 1062–1072. [[CrossRef](#)]
- Wang, J.; Kuang, C.; Chen, K.; Fan, D.; Qin, R.; Han, X. Wave current interaction by Typhoon Fongwong on saline water intrusion and vertical stratification in the Yangtze River Estuary. *Estuar. Coast. Shelf Sci.* **2022**, *279*, 108138. [[CrossRef](#)]
- Wang, Z.; Goodman, L. The evolution of a thin phytoplankton layer in strong turbulence. *Cont. Shelf Res.* **2010**, *30*, 104–118. [[CrossRef](#)]
- Huisman, J.; Pham Thi, N.N.; Karl, D.M.; Sommeijer, B. Reduced mixing generates oscillations and chaos in the oceanic deep chlorophyll maximum. *Nature* **2006**, *439*, 322–325. [[CrossRef](#)]
- Zheng, G.; Tang, D. Offshore and nearshore chlorophyll increases induced by typhoon winds and subsequent terrestrial rainwater runoff. *Mar. Ecol. Prog. Ser.* **2007**, *333*, 61–74. [[CrossRef](#)]
- Zhao, H.; Tang, D.; Wang, D. Phytoplankton blooms near the Pearl River Estuary induced by Typhoon Nuri. *J. Geophys. Res. Ocean.* **2009**, *114*, 1–9. [[CrossRef](#)]
- Zhao, H.; Han, G.; Zhang, S.; Wang, D. Two phytoplankton blooms near Luzon Strait generated by lingering Typhoon Parma. *J. Geophys. Res. Biogeosci.* **2013**, *118*, 412–421. [[CrossRef](#)]
- Chen, J.; Chen, S. Estuarine and Coastal Challenges in China. *Mar. Geol. Front.* **2002**, *18*, 1–5. [[CrossRef](#)]
- Guo, W.; Yang, Y.; Gong, Z.; Hu, M. Variation of salinity, PH, dissolved oxygen and COD in Xiamen Bay during typhoon and rainstorm process. *Mar. Sci.* **2000**, *25*, 1–5. (In Chinese)
- Yu, J.; Tang, D.; Li, Y.; Huang, Z.; Chen, G. Increase in fish abundance during two typhoons in the South China Sea. *Adv. Space Res.* **2013**, *51*, 1734–1749. [[CrossRef](#)]
- Kawabata, Y.; Okuyama, J.; Asami, K.; Okuzawa, K.; Yoseda, K.; Arai, N. Effects of a tropical cyclone on the distribution of hatchery-reared black-spot *tuskfish* *Choerodon schoenleinii* determined by acoustic telemetry. *J. Fish Biol.* **2010**, *77*, 627–642. [[CrossRef](#)]
- Lassig, B.R. The effects of a cyclonic storm on coral reef fish assemblages. *Environ. Biol. Fishes* **1983**, *9*, 55–63. [[CrossRef](#)]
- Houde, E.D.; Bichy, J.; Jung, S. Effects of hurricane Isabel on fish populations and communities in Chesapeake Bay. In Proceedings of the Chesapeake Research Consortium, Edgewater, MD, USA, 1 January 2005; pp. 193–199.
- Qiu, Y.; Lin, Z.; Wang, Y. Responses of fish production to fishing and climate variability in the northern South China Sea. *Prog. Oceanogr.* **2010**, *85*, 197–212. [[CrossRef](#)]

22. Webster, P.J.; Curry, J.A.; Liu, J.; Holland, G.J. Response to Comment on “Changes in Tropical Cyclone Number, Duration, and Intensity in a Warming Environment”. *Science* **2006**, *311*, 1713. [CrossRef]
23. Mendelsohn, R.; Emanuel, K.; Chonabayashi, S.; Bakkensen, L. The impact of climate change on global tropical cyclone damage. *Nature Clim. Chang.* **2012**, *2*, 205–209. [CrossRef]
24. Yu, J.; Tang, D.; Chen, G.; Li, Y.; Huang, Z.; Wang, S. The positive effects of typhoons on the fish CPUE in the South China Sea. *Cont. Shelf Res.* **2014**, *84*, 1–12. [CrossRef]
25. Chuang, L.; Shieh, B.S.; Liu, C.; Lin, Y.; Liang, S. Effects of Typhoon Disturbance on the Abundances of Two Mid-Water Fish Species in a Mountain Stream of Northern Taiwan. *Zool. Res.* **2008**, *47*, 564–573. Available online: <https://zoolstud.sinica.edu.tw/Journals/47.5/564> (accessed on 14 February 2023).
26. Chang, N.; Shiao, J.; Gong, G. Diversity of demersal fish in the East China Sea: Implication of eutrophication and fishery. *Cont. Shelf Res.* **2012**, *47*, 42–54. [CrossRef]
27. Liang, J.; Wang, W.; Xu, H.; Zhou, Y.; Xu, K.; Zhang, H.; Lu, K. Diel and seasonal variation in fish communities in the Zhongjieshan marine island reef reserve. *Fish. Res.* **2020**, *227*, 105549. [CrossRef]
28. Schade, L.; Emanuel, K. The Ocean’s Effect on the Intensity of Tropical Cyclones: Results from a Simple Coupled Atmosphere–Ocean Model. *J. Atmos. Sci.* **1999**, *56*, 642–651. [CrossRef]
29. Liu, Z.; Xu, J.; Sun, C.; Wu, X. An upper ocean response to Typhoon Bolaven analyzed with Argo profiling floats. *Acta Oceanol. Sin.* **2014**, *33*, 90–101. [CrossRef]
30. Tang, R.; Shen, F.; Ge, J.; Yang, S.; Gao, W. Investigating typhoon impact on SSC through hourly satellite and real-time field observations: A case study of the Yangtze Estuary. *Cont. Shelf Res.* **2021**, *224*, 104475. [CrossRef]
31. Pan, J.; Huang, L.; Devlin, A.T.; Lin, H. Quantification of Typhoon-Induced Phytoplankton Blooms Using Satellite Multi-Sensor Data. *Remote Sens.* **2018**, *10*, 318. [CrossRef]
32. Chen, J.; Jiang, C.; Wu, Z.; Long, Y.; Deng, B.; Liu, X. Numerical Investigation of Fresh and Salt Water Distribution in the Pearl River Estuary during a Typhoon Using a Fully Coupled Atmosphere-Wave-Ocean Model. *Water* **2019**, *11*, 646. [CrossRef]
33. Jeon, J.; Tomita, T. Investigating the Effects of Super Typhoon HAGIBIS in the Northwest Pacific Ocean Using Multiple Observational Data. *Remote Sens.* **2022**, *14*, 5667. [CrossRef]
34. Ma, C.; Zhao, J.; Bin, A.; Sun, S.; Zhang, G.; Huang, W.; Wang, G. Assessing responses of phytoplankton to consecutive typhoons by combining Argo, remote sensing and numerical simulation data. *Sci. Total Environ.* **2021**, *790*, 148086. [CrossRef] [PubMed]
35. Groom, S.; Sathyendranath, S.; Ban, Y.; Bernard, S.; Brewin, R.; Brotas, V.; Brockmann, C.; Chauhan, P.; Choi, J. Satellite Ocean Colour: Current Status and Future Perspective. *Front. Mar. Sci.* **2019**, *6*, 485. [CrossRef] [PubMed]
36. Banzon, V.; Smith, T.M.; Chin, T.M.; Liu, C.Y.; Hankins, W. A long-term record of blended satellite and in situ sea-surface temperature for climate monitoring, modeling and environmental studies. *Earth Syst. Sci. Data* **2016**, *8*, 165–176. [CrossRef]
37. Le Traon, P.Y.; Reppucci, A.; Fanjul, E.A.; Aouf, L.; Behrens, A.; Belmonte, M.; Bentamy, A.; Bertino, L.; Brando, V.E.; Kreiner, M.B.; et al. From Observation to Information and Users: The Copernicus Marine Service Perspective. *Front. Mar. Sci.* **2019**, *6*, 234. [CrossRef]
38. Cai, L.; Zhou, M.; Liu, J.; Tang, D.; Zuo, J. HY-1C observations of the impacts of islands on suspended sediment distribution in Zhoushan Coastal Waters, China. *Remote Sens.* **2020**, *12*, 1766. [CrossRef]
39. Liu, X.; Sun, L.; Yang, Y.; Zhou, X.; Chen, T. Cloud and Cloud Shadow Detection Algorithm for Gaofen-4 Satellite Data. *Acta Optica Sin.* **2019**, *39*, 438–449. [CrossRef]
40. Prakash, G.; Deng, L.; Nie, J. Effect of Image Fusion on Vegetation Index Quality—A Comparative Study from Gaofen-1, Gaofen-2, Gaofen-4, Landsat-8 OLI and MODIS Imagery. *Remote Sens. Environ.* **2020**, *12*, 1550. [CrossRef]
41. Cai, L.; Tang, D.; Levy, G.; Liu, D. Remote sensing of the impacts of construction in coastal waters on suspended particulate matter concentration—The case of the Yangtze River delta, China. *Int. J. Remote Sens.* **2016**, *37*, 2132–2147. [CrossRef]
42. Chin, T.M.; Vazquez-Cuervo, J.; Armstrong, E.M. A multi-scale high-resolution analysis of global sea surface temperature. *Remote Sens. Environ.* **2017**, *200*, 154–169. [CrossRef]
43. Wang, S.; Zhao, Y.; Yin, X.; Qiao, F. Current Status of Global Ocean Reanalysis Datasets. *Adv. Earth Res.* **2018**, *33*, 794–807. (In Chinese) [CrossRef]
44. Wang, H.; You, Z.; Guo, H.; Zhang, W.; Xu, P.; Ren, K. Quality Assessment of Sea Surface Salinity from Multiple Ocean Reanalysis Products. *J. Mar. Sci. Eng.* **2023**, *11*, 54. [CrossRef]
45. Wang, T.; Liu, G.; Gao, L.; Zhu, L.; Li, D. Biological responses to nine powerful typhoons in the East China Sea. *Reg. Environ. Chang.* **2017**, *17*, 465–476. [CrossRef]
46. Cai, L.; Tang, R.; Yan, X.; Zhou, Y.; Jiang, J.; Yu, M. The spatial-temporal consistency of chlorophyll-a and fishery resources in the water of the Zhoushan archipelago revealed by high resolution remote sensing. *Front. Mar. Sci.* **2022**, *9*, 2053. [CrossRef]
47. Price, J.F.; Sanford, T.B.; Forristall, G.Z. Forced Stage Response to a Moving Hurricane. *J. Phys. Oceanogr.* **1994**, *24*, 233–260. [CrossRef]
48. Zhao, H.; Shao, J.; Han, G.; Yang, D.; Lv, J. Influence of Typhoon Matsa on Phytoplankton Chlorophyll-a in the Northwest Pacific Ocean Offshore and Alongshore. *PLoS ONE* **2015**, *10*, e0137863. [CrossRef]

49. Han, G.; Ma, Z.; Chen, N. Hurricane Igor impacts on the stratification and phytoplankton bloom over the Grand Banks. *J. Mar. Syst.* **2012**, *100*, 19–25. [[CrossRef](#)]
50. Yin, W.; Ma, Y.; Wang, D.; He, S.; Huang, D. Surface Upwelling off the Zhoushan Islands, East China Sea, from Himawari-8 AHI Data. *Remote Sens.* **2022**, *14*, 3261. [[CrossRef](#)]
51. Yang, X.; Tang, D. Location of sea surface temperature cooling induced by typhoon in the South China Sea. *J. Trop. Oceanogr.* **2010**, *29*, 26–31. [[CrossRef](#)]
52. Behrenfeld, M.J.; Falkowski, P.G. Photosynthetic rates derived from satellite-based chlorophyll concentration. *Limnol. Oceanogr.* **2003**, *42*, 1–20. [[CrossRef](#)]
53. Guo, X.; Miyazawa, Y.; Yamagata, T. The Kuroshio Onshore Intrusion along the Shelf Break of the East China Sea: The Origin of the Tsushima Warm Current. *J. Phys. Oceanogr.* **2006**, *36*, 2205–2231. [[CrossRef](#)]
54. Lin, J.; Yan, Q.; Zhu, J.; Gong, F. Analysis of thermocline and hypoxia off the Changjiang Estuary in late summer. *J. Fish. Chin.* **2014**, *38*, 1747–1757. (In Chinese)
55. Yuan, J.; Liu, C. Improved scheme of axisymmetric typhoon bogus model its impact on numerical simulation of No. 0425 Typhoon. *J. Trop. Meteorol.* **2007**, *13*, 181–184.
56. Yang, Y.; Xian, T.; Sun, L.; Fu, Y.; Xun, S. Impacts of sequential typhoons on sea surface temperature and sea surface height in September 2008. *Acta Oceanol. Sin.* **2012**, *34*, 71–78. (In Chinese)
57. Sheng, J.; Zhai, X.; Greatbatch, R. Numerical study of the storm-induced circulation on the Scotian Shelf during Hurricane Juan using a nested-grid ocean model. *Prog. Oceanogr.* **2006**, *70*, 233–254. [[CrossRef](#)]
58. Wu, R.; Li, C. Upper ocean response to the passage of two sequential typhoons. *Deep Sea Res. Part I Oceanogr. Res. Pap.* **2018**, *132*, 68–79. [[CrossRef](#)]
59. Ding, Z. Influences of wind on vertical structures of temperature and salinity, and upwelling off Zhejiang coast in summer. *Chin. J. Oceanol. Limnol.* **1985**, *3*, 109–117. [[CrossRef](#)]
60. Zhang, H.; Liu, X.; Wu, R.; Chen, D.; Zhang, D.; Shang, X.; Wang, Y.; Song, X.; Jin, W.; Yu, L.; et al. Sea surface current response patterns to tropical cyclones. *J. Mar. Syst.* **2020**, *208*, 103345. [[CrossRef](#)]
61. Sun, L.; Li, Y.; Yang, Y.; Wu, Q.; Chen, X.; Li, Q.; Li, Y.; Xian, T. Effects of super typhoons on cyclonic ocean eddies in the western North Pacific: A satellite data-based evaluation between 2000 and 2008. *J. Geophys. Res. Atmos.* **2014**, *119*, 5585–5598. [[CrossRef](#)]
62. Gong, X.; Shi, J.; Gao, H.; Yao, X. Steady-state solutions for subsurface chlorophyll maximum in stratified water columns with a bell-shaped vertical profile of chlorophyll. *Biogeosciences* **2015**, *12*, 905–919. [[CrossRef](#)]
63. Oliveira, P.B.; Nolasco, R.; Dubert, J.; Moita, T.; Peliz, Á. Surface temperature, chlorophyll and advection patterns during a summer upwelling event off central Portugal. *Cont. Shelf Res.* **2009**, *29*, 759–774. [[CrossRef](#)]
64. Zhou, W.; Yin, K.; Harrison, P.J.; Lee, J.H.W. The influence of late summer typhoons and high river discharge on water quality in Hong Kong waters. *Estuar. Coast. Shelf Sci.* **2012**, *111*, 35–47. [[CrossRef](#)]
65. Pennock, J.R. Chlorophyll distributions in the Delaware estuary: Regulation by light-limitation. *Estuar. Coast. Shelf Sci.* **1985**, *21*, 711–725. [[CrossRef](#)]
66. Ritchie, J.C.; Cooper, C.M.; Schiebe, F.R. The relationship of MSS and TM digital data with suspended sediments, chlorophyll, and temperature in Moon Lake, Mississippi. *Remote Sens. Environ.* **1990**, *33*, 137–148. [[CrossRef](#)]
67. Diez-Minguito, M.; Swart, H.E. Relationships Between Chlorophyll-a and Suspended Sediment Concentration in a High-Nutrient Load Estuary: An Observational and Idealized Modeling Approach. *J. Geophys. Res. Ocean.* **2020**, *125*, e2019JC015188. [[CrossRef](#)]
68. Mukherjee, S.; Chaudhuri, A.; Sen, S.; Homechaudhuri, S. Effect of Cyclone Aila on estuarine fish assemblages in the Matla River of the Indian Sundarbans. *J. Trop. Ecol.* **2012**, *28*, 405–415. [[CrossRef](#)]
69. Bierman, P.; Lewis, M.; Ostendorf, B.; Tanner, J. A Review of Methods for Analysing Spatial and Temporal Patterns in Coastal Water Quality. *Ecol. Indic.* **2009**, *11*, 103–114. [[CrossRef](#)]
70. Huot, Y.; Babin, M.; Bruyant, F.; Grob, C.; Twardowski, M.S.; Claustre, H. Does chlorophyll a provide the best index of phytoplankton biomass for primary productivity studies? *Biogeosci. Discuss.* **2007**, *4*, 707–745. [[CrossRef](#)]
71. Bacher, C.; Grant, J.; Fang, J.; Zhu, M.; Besnard, M. Modeling the effect of food depletion on scallop growth in Sungo Bay (China). *Aquat. Living Resour.* **2003**, *16*, 10–24. [[CrossRef](#)]
72. Switzer, T.S.; Winner, B.L.; Dunham, N.M.; Whittington, J.A.; Thomas, M. Influence of sequential hurricanes on nekton communities in a Southeast Florida estuary: Short-term effects in the context of historical variations in freshwater inflow. *Estuaries Coasts* **2006**, *29*, 1011–1018. [[CrossRef](#)]
73. Lin, L.; Shen, J.; Zhang, J.; Wu, H. Storm surge of Typhoon Saomai and its effect on the stow net fishing. *Mar. Environ. Res.* **2007**, *105*, 537–540. (In Chinese)
74. Simon, N.S. Nitrogen cycling between sediment and the shallow-water column in the transition zone of the Potomac River and Estuary. II. The role of wind-driven resuspension and adsorbed ammonium. *Estuar. Coast. Shelf Sci.* **1989**, *26*, 483–497. [[CrossRef](#)]
75. Oyadomari, J.K.; Auer, N.A. Transport and growth of larval cisco (*Coregonus artedii*) in the Keweenaw Current region of Lake Superior. *Can. J. Fish. Aquat. Sci.* **2008**, *65*, 1447–1458. [[CrossRef](#)]
76. Zhang, Z. The relationship between typhoons and fisheries. *J. Aquac.* **1992**, *3*, 29–30. (In Chinese)

77. Yu, J.; Chen, B.; Chen, Z.; Huang, Z. The impacts of typhoon “Kai-tak” on fishery in west Guangdong fishing ground. *Mar. Environ. Res.* **2015**, *34*, 411–419. [[CrossRef](#)]
78. Greenwood, M.F.D.; Stevens, P.W.; Matheson, R.E. Effects of the 2004 hurricanes on the fish assemblages in two proximate southwest Florida estuaries: Change in the context of interannual variability. *Estuaries Coast.* **2006**, *29*, 985–996. [[CrossRef](#)]

Disclaimer/Publisher’s Note: The statements, opinions and data contained in all publications are solely those of the individual author(s) and contributor(s) and not of MDPI and/or the editor(s). MDPI and/or the editor(s) disclaim responsibility for any injury to people or property resulting from any ideas, methods, instructions or products referred to in the content.